JOURNAL OF PROPULSION AND POWER
Vol. 25, No. 3, May–June 2009

# Swept-Leading-Edge Pylon Effects on a Scramjet Pylon-Cavity Flameholder Flowfield

Andrew B. Freeborn* and Paul I. King†
*Air Force Institute of Technology, Wright–Patterson Air Force Base, Ohio 45433*
and
Mark R. Gruber‡
*U.S. Air Force Research Laboratory, Wright–Patterson Air Force Base, Ohio 45433*

DOI: 10.2514/1.39546

**This study explores the effect of adding a pylon to the leading edge of a cavity flameholder in a scramjet combustor. Data were obtained through a combination of wind-tunnel experimentation and steady-state computational fluid dynamics. Wind-tunnel data were collected using surface pressure taps, static and total probe data, shadowgraph flow visualization, and particle image velocimetry. Computational fluid dynamics models were solved using the commercial FLUENT software. The addition of an intrusive device to the otherwise low-drag cavity flameholder offers a potential means of improving combustor performance by enabling combustion products to propagate into the main combustor flow via the low-pressure region behind the pylon. This study characterized the flowfield effects of adding the pylon as well as the effect of changing Reynolds numbers over the range of approximately $33 \times 10^6$ to $55 \times 10^6$ $m^{-1}$ at a Mach number of 2. The addition of the pylon resulted in approximately 3 times the mass flow passing through the cavity compared with the cavity with no pylon installed. Reynolds number effects were weak. The addition of the pylon led to the cavity fluid traveling up to the top of the pylon wake and significantly increasing the exposure and exchange of cavity fluid with the main combustor flow.**

## Nomenclature

| | | |
|---|---|---|
| $D$ | = | cavity depth |
| $h$ | = | pylon height |
| $L$ | = | cavity length |
| $M$ | = | Mach number |
| $\dot{m}$ | = | mass flow |
| $P_t$ | = | stagnation-tank pressure |
| $p$ | = | local static pressure |
| $p_{\text{ref}}$ | = | reference pressure |
| $q$ | = | dynamic pressure |
| $U$ | = | mean flow speed |
| $u_f$ | = | flame speed |
| $u_{y+}$ | = | velocity in the positive $y$ direction |
| $w$ | = | pylon width |
| $x$ | = | streamwise coordinate |
| $y$ | = | vertical coordinate |
| $z$ | = | cross-stream coordinate |
| $\rho$ | = | density |

## I. Introduction

HYPERSONIC flight powered by scramjet engines is an active area of research and development today, as illustrated by the variety of programs underway to explore this flight regime in the United States and other countries around the world [1–5]. One important aspect concerns flameholding and fuel distribution. Combustion must occur within a very short time in a scramjet combustor. Flameholders can aid ignition and flame-spreading within the flow by providing distributed, stable energy sources. Wall-based flameholders (e.g., cavities) enable the engine to sustain combustion with less drag than in-stream devices, resulting in a shorter and lighter engine. However, wall-based flameholder products tend to remain near the combustor wall [6]. Intrusive devices or fuel-injection schemes near the cavity leading edge can carry combustion products away from the cavity and into the core combustor flow, but less is known about optimizing this combination. Motivated by previous studies at the Air Force Institute of Technology (AFIT) and the U.S. Air Force Research Laboratory (AFRL) [6–9], this paper discusses a combined computational and experimental study of a pylon positioned on the upstream edge of a cavity flameholder. The study characterizes flow interactions between the pylon and an inclined cavity to more effectively take advantage of the unique flow characteristics of the pylon-cavity flowfield in future combustor work. Data analysis considered the entire span of the cavity rather than focusing on centerline results. Variation of Reynolds number provided an initial look at the effect of changing design points or scale. Figure 1 illustrates the pylon-cavity test article.

## II. Background

Ignition of fuel within an engine requires appropriate temperature, pressure, equivalence ratio, and sufficient residence time for combustion to occur. A flameholder minimizes the ignition delay time, and therefore combustor length, required for initiating and sustaining combustion within the engine [10]. Any component providing a zone with a flow velocity small enough for effective mixing and for the flame to stabilize can work as a flameholder. Common flameholders include the $v$ gutter commonly found in turbine afterburners or a simple step. Flameholders provide a turbulent recirculation region in which combustion can take place with fuel and air entrained from the main flow. If the recirculation region entrains an appropriate fuel–air mixture, a stable flame should burn and provide a constant ignition source.

Cavity flameholders present a potential flameholding solution by creating a relatively low drag recirculation region in which fuel and

Presented as Paper 4709 at the 44th AIAA/ASME/SAE/ASEE Joint Propulsion Conference, Hartford, CT, 20–23 July 2008; received 3 July 2008; revision received 24 November 2008; accepted for publication 22 December 2008. 

*Ph.D. Candidate; currently Deputy Director of Education, U.S. Air Force Test Pilot School, 220 South Wolfe Avenue, Edwards Air Force Base, CA 93524; andrew.freeborn@edwards.af.mil. Senior Member AIAA.
†Professor, Department of Aeronautics and Astronautics, 2950 Hobson Way; paul.king@afit.edu. Senior Member AIAA.
‡Senior Aerospace Engineer, Propulsion Sciences Branch, 1950 Fifth Street; mark.gruber@wpafb.af.mil. Associate Fellow AIAA.

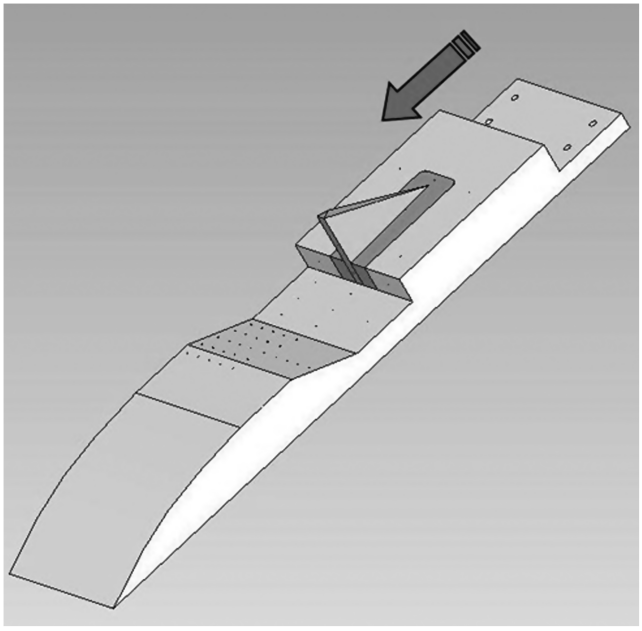

**Fig. 1 Pylon-cavity test article.**

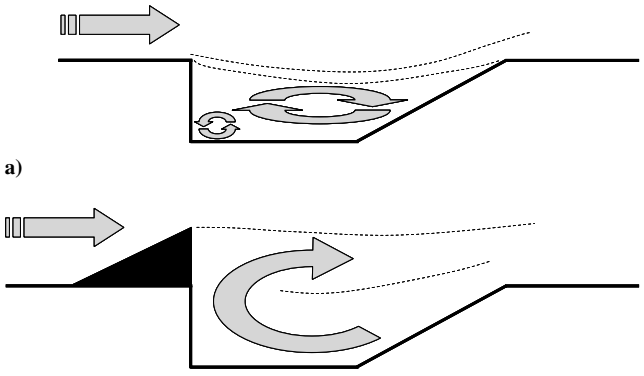


**Fig. 2 Representation of centerline flow in an inclined-cavity flameholder: a) without leading-edge pylon and b) with leading-edge pylon.**

air can react and generate a stable flame. Both step and cavity flameholders rely on recirculation behind a discontinuous step in the combustor surface. However, step designs suffer from higher drag and stagnation pressure losses than cavities [10]. Also, total temperature within the cavity can approach the freestream total temperature, allowing the cavity flameholder to take better advantage of the energy in the oncoming flow [11]. Without a flameholder, combustor length would need to account for the ignition delay time of the fuel. Hydrocarbon fuel ignition in a supersonic combustor may take a significant distance because the ignition delay of hydrocarbon fuels is on the order of 1 ms [12]. Thrust-to-drag ratio is roughly proportional to the ratio of combustor diameter and combustor length, making shorter engines highly desirable [13]. Cavity residence times equal to or greater than the ignition delay permit a stable flame to exist within the flameholder, enabling a shorter combustor.

Cavity flows can be classified as either open or closed, based primarily on cavity length-to-depth ratio $L/D$. A shear layer forming at the leading edge of the cavity and reattaching on the downstream wall of the cavity characterizes open cavity flow. The shear layer over a closed cavity, on the other hand, reattaches to the floor of the cavity. Significantly higher drag results from the flow encountering the downstream wall in closed cavities, favoring the use of open cavities as flameholders. The actual transition from open to closed cavity depends on the overall flow, but typically occurs as the $L/D$ increases past 10 [10]. Some of the factors influencing the cavity flow include geometry and freestream Mach number [14]. The incoming boundary layer will influence the shear layer that forms above the cavity, but otherwise, Reynolds number has a minimal effect on cavity-only flows.

Cavity shape has probably the strongest effect on cavity flow characteristics. Rectangular cavities are prone to unsteady flow due to acoustic disturbances caused by the shear layer impinging on the downstream wall and by periodic mass exchange with the main flow as the disturbed shear layer moves up and down [15,16]. Inclining the downstream wall, as seen in Fig. 2a, allows the shear layer to smoothly reattach, thereby reducing the magnitude of the unsteady effects associated with rectangular cavities [10,13,15,17]. However, even with an inclined downstream wall, oscillations remain possible [18,19]. Other effects within the cavity may further reduce unsteady fluctuations. For instance, fuel injection upstream of the cavity reduces cavity instability [20]. Additionally, heat addition due to combustion may suppress cavity instabilities seen under cold-flow conditions [21,22].

In addition to reducing pressure fluctuations, inclining the downstream wall results in slightly increased drag and mass exchange rate [17,23]. Inclining the downstream wall exposes more of the downstream wall to the oncoming flow increasing drag. Combusting flow should partially offset this added drag because the shear layer grows and the top of the shear layer rises in combusting flow [24,25]. A large vortex oriented spanwise across the cavity dominates inclined-cavity flow and governs mass exchange between the cavity and main flow. A smaller counter-rotating vortex may form along the bottom of the upstream cavity wall [17,18,23]. These vortices provide a zone for the fuel–air mixture to ignite and form a stable flame. Ongoing research has examined these vortices in an attempt to improve flameholding and ensure sufficient cavity residence time to counter the increased mass exchange driven by inclining the downstream cavity wall [11,17,23]. The overall flow in the cavity may appear to be dominated by two-dimensional effects, but the flow remains three-dimensional. Streamwise vortex structures form off the side wall, producing nonuniform pressures along the downstream wall. This effect was computationally presented in [15] and also noted in an experimental injection study in [11]. References [17,23] also presented an inverse relationship between cavity mass exchange and cavity residence time. For the flameholder to function effectively, residence time must remain high enough for a stable flame to burn in the flameholder, yet sustain sufficient mass exchange to provide a steady source of fresh air and/or fuel. Cavity flameholders and the recirculation region of step flameholders tend to become fuel-rich, or at least contain significant fuel-rich regions [17,26,27], highlighting the importance of balancing sufficient mass exchange with the main flow and the increased residence time required for hydrocarbon combustion.

The goal of a cavity flameholder is to increase the residence time of the fuel–air mixture and reduce engine length and drag. Open cavities, such as the one under study, tend to have less mass exchange with the main flow than closed cavities [17]. Cavity shape alone appears to have little effect on residence time or mass entrainment [23]. Residence time is primarily driven by cavity depth, because deeper cavities have a larger volume and therefore contain more mass for a given density. Longer cavities also have increased volume, which increases residence time, but higher mass exchange due to the larger area exposed to the freestream flow decreases residence time. As a result, length has little effect on residence time. The inclined cavity has lower residence times compared with rectangular cavities of the same $L/D$ ratio, due to higher entrainment caused by the shear layer moving lower into the cavity [17,23].

Though cavity flameholders can provide a steady source of ignition, cavity combustion products generally remain near the floor of the combustor. Assuming a uniform and suitable equivalence ratio and a main flow parallel to the cavity, the flame spread in natural flame convection can be estimated by

$$\text{spread angle} = \sin^{-1}\left(\frac{u_f}{U}\right) \quad (1)$$

where $u_f$ is the turbulent flame speed and $U$ is the flow speed. For example, a typical hydrocarbon turbulent flame speed is about 4.5 m/s (about an order of magnitude above the laminar flame speed) [12]. In a 500 m/s flow, the spread angle is about a half-degree. Thus, even with effective flameholding the flame will remain near the combustor wall, as seen in previous research [6].

Intrusive devices can enhance the interaction between a cavity-based flameholder and a fuel–air mixture in the core flow [6–9,28]. A pylon placed at the leading edge of the cavity provides such a mechanism by increasing mass exchange between the cavity and freestream [29–31] and improving mixing due to pylon vortex/shock interactions [32,33]. Low pressure behind the pylon draws fluid out of the higher pressure cavity and into the pylon wake, enabling increased mass exchange between the cavity and main flow, compared with a cavity-only case [28,31] (see Fig. 2b). Supersonic expansion at the pylon edges results in low pressure behind the pylon [34]. The pressure differential between the cavity and downstream pylon face results in a flow of cavity fluid upward behind the pylon. This upward flow lies between a pair of streamwise counter-rotating vortices formed as the flow over the top of the pylon spills over each side. The vortices generated by a ramp fuel injector produce a similar effect [25,35]. This additional streamwise vorticity should enhance mixing between the pylon wake and main flow [25,36].

Although using pylons to specifically induce flow out of a cavity flameholder has only recently been explored [28,31], pylons, ramps, and struts as combustor enhancements with and without associated cavity flameholders have been the focus of several research efforts [7–9,32,33,37–39]. More specifically, [7,9,33,38] demonstrated improved fuel penetration and mixing of wall-injected fuel into the low-pressure region behind small pylons upstream of the fuel injectors. In addition to the improved penetration of fuel into the main combustor flow, these studies noted improved mixing due to axial vorticity shed off the pylons. Complementing improved penetration and mixing behind the pylons, the addition of small pylons (approximately 1 cm high) with sharp leading edges ahead of fuel injectors, as described in [33], showed no significant additional total pressure losses. Pylon fuel injection ahead of step flameholders has also been shown to sustain combustion [40]. Reference [41] explored the use of wedge fuel injectors alone or ahead of a cavity and showed improved combustion characteristics with the wedge injector positioned at the leading edge of a cavity flameholder.

Increased mass exchange tends to reduce overall residence time in the cavity, resulting in a design limitation for the designer, because it may drive the operating and ignition envelope [17,28]. The increased mass exchange due to the pylon has an effect similar to increasing the length of an open inclined cavity [23], but much more pronounced due to the intrusive interaction of the pylon with the main flow [31]. The improved penetration of flameholder products into the main flow will enable the use of a larger volume of the main flow for combustion, although reduced residence time must be accounted for. Reacting flow will counter this decreased residence time to some degree [17]. Drag is a concern; however, static pressure rise due to combustion behind the pylon should at least partially offset the pressure drag increase from adding the pylon to the cavity flameholder [32].

Experimental data in [42] showed that adding a strut ahead of a cavity flameholder resulted in more stable combustion. The increased mass exchange due to the pylon-induced flow should also contribute to steadier flow, because mass can leave the cavity behind the pylon at a nearly constant rate instead of through the shear layer oscillating up and down at the rear of the cavity. Even small rectangular spoilers placed spanwise ahead of a cavity disturbed the flow approaching the cavity, resulting in significantly reduced pressure fluctuations in a rectangular cavity, although oscillation frequencies were unaffected [16]. Reference [43] noted possible oscillations of the shear layer near the ramps of a ramp mixer ahead of a step flameholder. Therefore, it seems reasonable that fluctuations may remain after the addition of a pylon to the cavity flameholder, although at a reduced magnitude.

The pylon wake and cavity shear layer will interact. The shear layer should progressively grow out of the cavity in the vicinity of the wake due to the lower-velocity pylon wake. This combined pylon wake and cavity shear layer will present a larger interface between the oncoming flow and flameholder products than a cavity flameholder without the pylon. Extrapolating from [7], by transporting fuel-rich combustion products from within the cavity, there may be a larger region above the cavity with suitable conditions for combustion. Reference [7] noted that the pylon ahead of the cavity configuration may also lift the shear layer. Additionally, the shocks off the pylon may further enhance mixing in the shear layer as they reflect off the duct walls and over the cavity [25].

Adding a pylon to a cavity flameholder will create shocks within the combustor section of the engine. An oblique or bow shock will form off the leading edge of the pylon reflecting off the duct ceiling and wall. Expansion waves will form at the back of the pylon. The pylon waves and reflections will interact with the waves due to the cavity, resulting in a complex three-dimensional flowfield downstream of the pylon. Because shocks are an inevitable result of using a pylon with the cavity flameholder, the shock system in a final design should be located to enhance mixing in the flameholder and throughout the combustor section.

Adding a pylon to a cavity-based flameholder should enhance the interaction between the cavity and a fuel–air mixture in the main combustor flow. Knowledge of the particular characteristics of the overall pylon-cavity flow will provide a previously unavailable tool for scramjet researchers to enhance the effectiveness of scramjet combustor designs.

## III. Wind-Tunnel Facility and Instrumentation

### A. AFIT 6 × 6 in. Supersonic Wind Tunnel

Testing was accomplished in the AFIT 6 × 6 in. supersonic wind tunnel. The tunnel is a blowdown-type tunnel built by Aerolab, capable of Mach numbers from 1.4 to 4.0. A lower sliding-block nozzle with contours based on [44] provides the ability to adjust the Mach number. Air for the tunnel is stored in a 22.7 kl tank at up to 1380 kPa and provided by two 37.3 kW compressors (Ingersoll-Rand UP6-50PE-200) with two desiccant-type dryers (Donaldson AHLD-350). Dew point measured downstream of the dryers is below −40°C. A perforated steel disc inside the upstream end of the stagnation tank evenly distributes the supply flow across the stagnation tank. Additionally, three stainless steel screens installed in the stagnation tank enhance flow uniformity [45]. A pressure regulator installed immediately upstream of the stagnation tank held tank pressures to within approximately 2% of target pressure. Conditions were considered stable for data collection when stagnation pressure $P_t$ was within 10% of peak pressure for each run. Stable run times varied with stagnation pressure from approximately 15 s at $P_t = 248.2$ kPa to approximately 8 s at $P_t = 427.5$ kPa with $M = 2$. Supply temperature was not controllable and varied between approximately 260 and 300 K over the course of the study. Stagnation temperature and Reynolds number varied approximately ±3% during data runs.

### B. Test Section and Flameholder Model

We modified the original wind tunnel by inserting a new, more accessible, test section downstream of the original test section. The test section is an 86.4-cm-long constant-area duct with internal dimensions of 15.2 × 16.5 cm. The test section has optical access through the top and both sides. A removable side window allows installation of mounting hardware for probe measurements. The test-section floor accommodates access to the test article for surface pressure tap tubing, pressure transducer wiring, and particle image velocimetry (PIV) seeding.

The test-article geometry builds on previous work at AFIT and AFRL [6–9,11,17,24] and was selected to clearly show the various flow features, but not optimally designed to minimize losses. The

downstream face of the pylon is flush with the cavity step and rectangular in shape, resulting in a flat triangular top face, as shown Fig. 3. This design provides a simple geometry to study flow traveling from the cavity into the core flow. The cavity depth $D$ is 2.5 cm and length $L$ is 10.2 cm. Cavity length is measured from the leading edge of the cavity to the midpoint of the aft ramp. The test-section duct is 15.2 cm wide and 16.5 cm high. The pylon, when installed, is 5.1 cm high and 10.2 cm long and 1.0 cm wide. Cavity length-to-depth ratio $L/D$ is 4.0, pylon height-to-cavity-depth ratio $h/D$ is 2.0, and pylon width-to-depth ratio $w/D$ is 0.4. The aft ramp is inclined 22 deg from the horizontal and the pylon is swept back 29 deg from horizontal. Ongoing combustion research at AFRL uses a similar pylon-cavity flameholder with $h/D = 1.5$ and $w/D = 0.6$ [28]. Forty 0.8-mm-diam pressure taps were located at several locations to measure the surface pressure in and around the flameholder. Figure 4 illustrates the locations of the pressure taps as well as the port used for either a flush-mounted pressure transducer or mounting a PIV injector.

The coordinate system associated with the test article centers on the leading edge of the cavity at the base of the pylon and is depicted in Fig. 4.

### C. Instrumentation

Wind-tunnel monitoring used a locally developed LabVIEW program. Pressure monitoring used Endevco piezoelectric pressure transducers. The pressure transducers were calibrated to local atmospheric pressure once, or more, daily using a resonant sensor barometer (Druck, Inc. DPI-141), accurate to $\pm 25.5$ Pa. All pressure transducers were calibrated to $\pm 68.9$ Pa. Exposed, beaded-tip, K-type thermocouples (Watlow ACEF00Q060EK000) placed in the supply channel and stagnation chamber provided temperature data accurate to $\pm 2.2$°C. A data acquisition system collected data at 20 Hz (National Instruments SCXI-1000 chassis, SCXI-1600 USB data acquisition and control module, SCXI-1112 thermocouple input module, and two SCXI-1121 isolation amplifier modules).

Shadowgraph data were collected using a Photron Fastcam-X color high-speed camera system with a Tokina 80–200 mm lens at an $f$ stop of 4. All captured images used an exposure time of $1.5625 \times 10^{-5}$ s $(1/64,000$ s). The system was independently controlled from a standalone personal computer. The Fastcam system supports video capture at up to 16,000 frames per second. Full-frame video ($1280 \times 1024$ pixels) was available at up to 500 frames per second and used for imaging the overall flow. Frame size became increasingly limited at the higher frame rates ($320 \times 32$ pixels at 16,000 frames per second).

Average surface pressure data were collected using a pressure scanning system with a 206.8 kPa differential pressure scanner (Esterline Pressure Systems DTC Initium 64HD-0803001000) and supporting hardware, controlled independently of other lab systems on a personal computer. The pressure scanner accuracy of 0.1% of full scale equated to $\pm 206.8$ Pa. The scanner operated at approximately 8.5 Hz using 41 channels. Surface pressure taps were connected to the scanner using 1.6 mm (o.d.) metal tubing mounted beneath each tap and approximately 60 cm of 1.5 mm (i.d.) plastic tubing and associated fittings.

A Dantec Dynamics DC PIV system provided PIV data. The light sheet was created using a New Wave Research SOLO200XT dual-

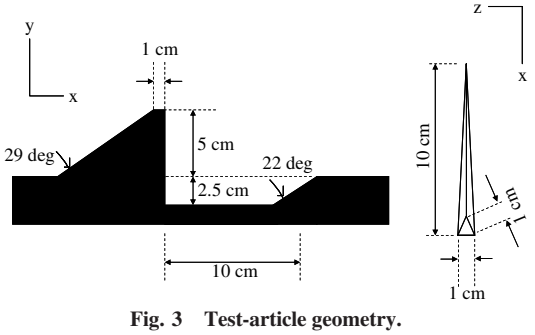


**Fig. 3 Test-article geometry.**

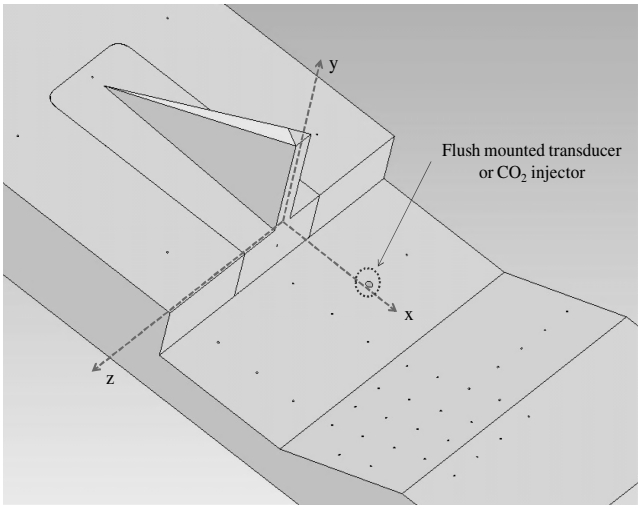


**Fig. 4 Pressure tap placement and coordinate system.**

flash-lamp-pumped Nd:YAG laser emitting a 532 nm beam. Dantec Dynamics model $80 \times 70$ light sheet optics mounted to a model $80 \times 39$ mirror arm formed the laser sheet in the test section. The camera was a Dantec FlowSense 4M, using an AF Micro Nikkor 60 mm lens at an $f$ stop of 2.8. PIV system control and data reduction were accomplished on an independent personal computer running Dantec Dynamic Studio version 2.0. The system was capable of capturing 70 images pairs per run, but sparse seeding required up to 15 data runs for a single test condition. Flow seeding was accomplished using a $CO_2$/dry-ice clean-seeding method under development at AFIT [46–51]. This study used two different particle-seeding configurations. Two injector ports installed in the stagnation tank upstream of the tunnel nozzle provided seeding without disturbing the flow. The other injector configuration used a single stagnation-tank injector and an injector mounted to the cavity floor oriented toward the $+z$ wall of the cavity. Mounting an injector within the cavity disturbed the cavity flow, but provided the ability to seed the pylon wake for qualitative analysis. Particle sizes were not characterized in the $6 \times 6$ in. tunnel, however, relaxation times using the same $CO_2$ seeding system in a 40 $cm^2$ tunnel were on the order of 50 $\mu$s and consistent with 2-$\mu$m-diam particles [50].

## IV. Computational Approach

Steady-state computational data were obtained using FLUENT version 6.3.21 and mesh generation used GridGen version 15.11. A Linux cluster at AFIT, using up to 24 processors, provided a parallel computing environment for flow solutions. Validation was accomplished through comparison with wind-tunnel results.

For this study, the three-dimensional Favre-averaged Navier–Stokes equations were solved using a coupled, implicit, second-order upwind solver. Cell fluxes were computed using a Roe scheme and the viscosity was determined using Sutherland's law. The working fluid was air treated as an ideal gas with no reactions modeled, corresponding to the wind-tunnel conditions.

The $\kappa$-$\omega$ shear stress transport (SST) model [52] was used for turbulence modeling. The SST model combines the advantages of the $\kappa$-$\omega$ model near solid surfaces with the $\kappa$-$\varepsilon$ model, which has good free-shear-flow characteristics, making it well suited for this flow. The SST model also has improved performance in adverse pressure gradient flows over either the $\kappa$-$\omega$ or $\kappa$-$\varepsilon$ models. The SST model was used successfully in a previous AFRL study on cavity flow [23].

The solution was handled in two stages. First, the wind-tunnel nozzle was modeled up to the entrance of the test-section duct (see Fig. 5). Actual wind-tunnel stagnation-tank conditions populated the pressure inlet boundary condition at the nozzle inlet. Estimated average conditions for the nozzle exit based on wind-tunnel test-section measurements provided initial conditions at the outlet boundary. The converged outlet conditions for the tunnel nozzle were then stored and used as inlet conditions for the test section with

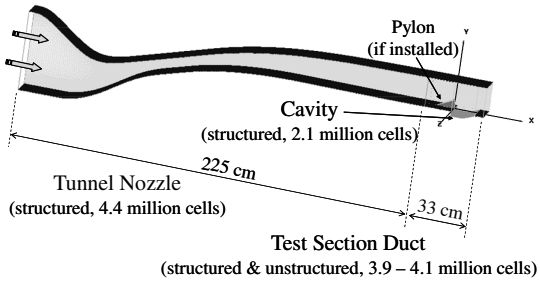


**Fig. 5 Computational domains.**

and without the pylon installed. Supersonic flow at the entrance and exit allowed the use of test-section inlet boundary conditions for the initialization of the test-section outlet. Wall boundaries were modeled as smooth, no-slip, adiabatic surfaces.

The computational domain shown in Fig. 5 consisted of several different meshes. The tunnel nozzle mesh was a structured grid of approximately 4.4 million cells. The cavity was an independent mesh and merged with the duct mesh within FLUENT. Using an independent cavity mesh ensured as much commonality between the pylon and no-pylon models as possible. The cavity mesh consisted of approximately 2.1 million cells. Two different test-section duct meshes were used. The no-pylon mesh consisted of approximately 3.9 million structured cells. The pylon model used a hybrid mesh consisting of approximately 3.6 million structured cells in three blocks surrounding approximately 550,000 unstructured cells surrounding the pylon. The cavity-pylon and cavity-only meshes used identical wall spacing and spacing above/below the cavity shear layer. The height of the first cell center above the test-section floor upstream of the cavity was $7.5 \times 10^{-5}$ m. The resulting $y+$ values of the first cell center averaged approximately 35 to 57, depending on Reynolds number, necessitating the use of wall functions to more accurately model the boundary layer. This spacing resulted in approximately 32 cells in the 2-cm-thick boundary layer near the test-section entrance at $x \approx -12$ cm. Comparison of the boundary layer entering the test section showed excellent agreement between CFD and PIV [31]. Course spacing along the tunnel ceiling conserved computational expense ($y+ \approx$600–1000). Convergence monitoring compared the difference between the inlet and outlet mass flow rates. As convergence was approached, this difference approached zero. As a secondary measure of convergence, the same check was made at the junction between the cavity and test-section duct. The solution was considered converged when the average error in mass flow for the duct decreased by 3 orders of magnitude. Acceptable convergence for all cases required less than 20,000 iterations and approximately 110 h per case.

## V. Results and Discussion

This section will present results of our cold-flow study, including flow visualization, pressure data, and general flowfield characteristics, and will end with a discussion of cavity mass exchange. Experimental and computational data were obtained at a test condition of $M = 2$ over a range of unit Reynolds number of approximately $33 \times 10^6$ to $55 \times 10^6$ m$^{-1}$. Results were obtained with the pylon installed ahead of the cavity flameholder as well as baseline data with the cavity flameholder only, providing a direct quantitative comparison of cavity-only flow with pylon-cavity flow. The cold-flow condition approximates the state of a combustor before initiating fuel flow. Additionally, whereas a reacting flow will alter the flowfield characteristics, such as enlarging the recirculation region size [26] or inhibiting cavity pressure/velocity fluctuations [21,22], the underlying flowfield structures may remain, as described in [53,54]. These cold-flow data provide a stepping-off point for further research in a reacting environment.

### A. Flow Visualization

Flow visualization using shadowgraph video provided a quick assessment of prominent flameholder structures as well as validation

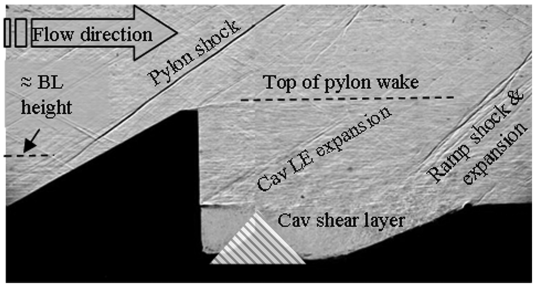


**Fig. 6 Shadowgraph image of significant features ($Re \approx 42 \times 10^6$ m$^{-1}$, $M = 2$, and unusable hatched area); BL denotes boundary layer, Cav denotes the cavity, and LE denotes the leading edge.**

of the CFD results. Figure 6 presents an instantaneous shadowgraph image of the pylon-cavity flameholder model at $Re \approx 42 \times 10^6$ m$^{-1}$ and was created by joining two images at the same stagnation pressure setting. The unusable hatched region in Fig. 6 is due to the overlap of the two circular fields of view. The flow is from the left and the prominent flow features agree with CFD density gradient results shown in Fig. 7 created by overlapping density gradient contours from four $z$ planes (light shading corresponds to decreasing density and dark shading to increasing density). The *zebra-striping* appearance between the pylon and ramp shocks in Fig. 7 results from overlapping density gradient data sets (centerline and 2, 4, and 6 cm offcenterline). The shadowgraph in Fig. 6 displays the second derivative of density ($d^2\rho/dx^2$), versus the density gradients ($d\rho/dx$) presented in Fig. 7, which emulates schlieren photography [55]. Prominent features visible in Fig. 6 include a shock off the leading edge of the pylon, a recompression shock forming off the downstream cavity ramp, and an expansion at the cavity leading edge. The cavity shear layer and pylon wake also appear in the image. The flow off the top of the pylon is more complex. The pylon wake in Fig. 6 appears to extend above the top of the pylon. Considering the CFD results of Fig. 8, the wake only extends above the pylon on the outside edges of the pylon base ($z \approx \pm -0.5$ cm), where the flow travels away from the wake at about a 45 deg angle between two sets of counter-rotating vortices. The wave feature angling upward off the top of the pylon in Fig. 6 is likely an expansion, because the flow actually turns slightly downward on the centerline. These structures compare qualitatively well with results presented in [28] for a similar test condition, although they used a different pylon and slightly divergent duct. No significant variation in these flow features was noted over the range of Reynolds numbers tested.

### B. Pressure Data

Surface pressures provide a means of estimating the shape and characteristics of the cavity shear layer impinging on the downstream ramp. The static pressure within the cavity directly affects reactions, and cavity surface pressure data provide a means of estimating the regions favorable or unfavorable for combustion, assuming an appropriate fuel–air mixture. Additionally, the use of CFD allowed for the estimation of overall average pressure effects. The measured pressure-coefficient results were computed using a reference surface pressure $p_{\text{ref}}$ from a pressure tap approximately 1 cm ahead of the pylon ($x = -11$ cm) and estimated dynamic pressure $q$ entering the test section.

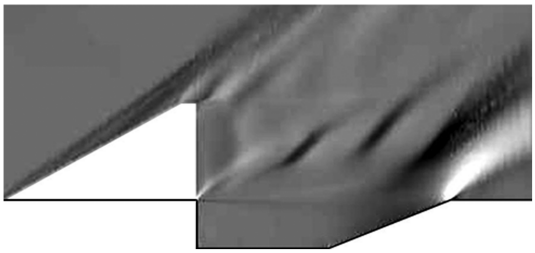

**Fig. 7 CFD simulated schlieren image (data from $z = 0$, 2, 4, 6 cm; grayscale of $\partial\rho/\partial x$; $Re \approx 42 \times 10^6$ m$^{-1}$, and $M = 2$).**

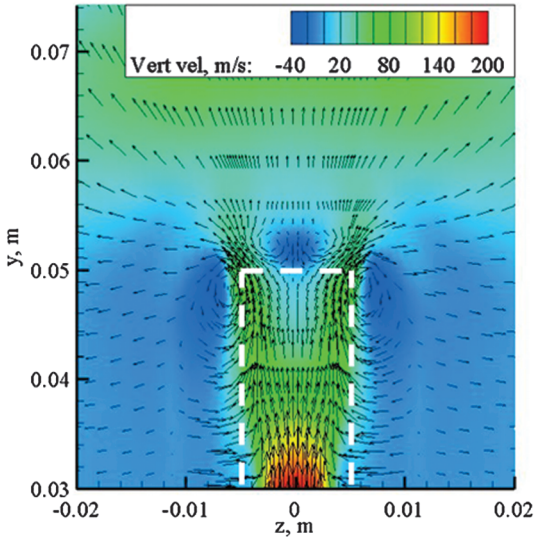


**Fig. 8 Flowfield 1 cm behind the top of the pylon (contours of vertical velocity; dashed line represents the pylon).**

Because wind-tunnel conditions varied from run to run, the pressure coefficient was usually used for comparative analysis. The pressure coefficient was computed as

$$C_p = \frac{p - p_{\text{ref}}}{q} \tag{2}$$

CFD enabled the calculation of the mass-averaged static pressure within the entire cavity ($y < 0$ cm) and showed a small pressure rise with the addition of the pylon (less than 2% at all Reynolds numbers). This pressure rise equated to an approximately 3% increase in average cavity pressure over the incoming duct static pressure. Considering simple Mach number versus area variation for comparison purposes, a step flameholder using the same inlet conditions and area change at the step would experience on the order of a 20% static pressure decrease. Higher average static pressure should contribute to better overall ignition and flameholding. However, just as important as average pressure within the flameholder are local pressures at various points within the cavity, as they can represent hot spots or regions that are unsuitable for combustion. The pressure environment along the floor and upstream edge of the cavity, where the flow is subsonic, was relatively unchanged with the addition of the pylon, as seen in the surface pressure results in Fig. 9.

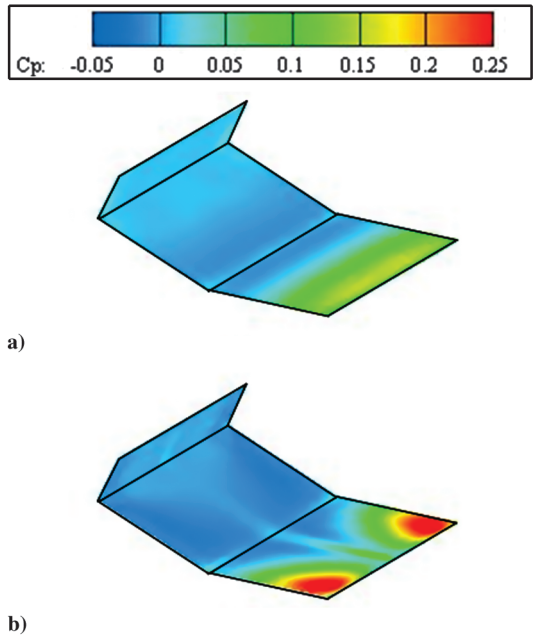


**Fig. 9 CFD cavity surface pressure coefficient: a) cavity only and b) cavity pylon.**

On the downstream ramp, computational surface pressure data for the cavity-only case show relatively uniform pressures along the lower half of the cavity ramp, with a gradual increase toward the top of the ramp (Fig. 9a). However, with the pylon installed, the surface pressure rises along the downstream ramp, but with relatively low pressure near the wake of the pylon and increasing pressure toward the walls, where the cavity shear layer impinges on the ramp (Fig. 9b). No significant Reynolds number effects on the surface pressure coefficients were noted. Figure 10 shows measured and predicted centerline surface pressures and shows generally good agreement between computational and tunnel results. However, at lower Reynolds numbers, the centerline pressure without the pylon in Fig. 10a rises higher on the downstream ramp than predicted and is associated with a small centerline velocity deficit in the incoming test-section flow. These no-pylon centerline data are consistent with cavity-only centerline pressures in [17]. With the pylon (Fig. 10b), measured centerline pressures along the downstream ramp appear to peak slightly upstream, compared with CFD, and suggest that the shear layer with the pylon installed may sit slightly lower on the ramp than predicted in the low Reynolds number case.

Two significant effects likely explain the high pressures on the top outboard corners of the cavity ramp. First, the extra mass drawn up behind the pylon draws a portion of the duct flow lower into the cavity, leading to a deeper impingement of the shear layer. Second, the recompression shock off the pylon wake interacts with the ramp shock above the outboard edges of the cavity ramp seen in Fig. 6. The

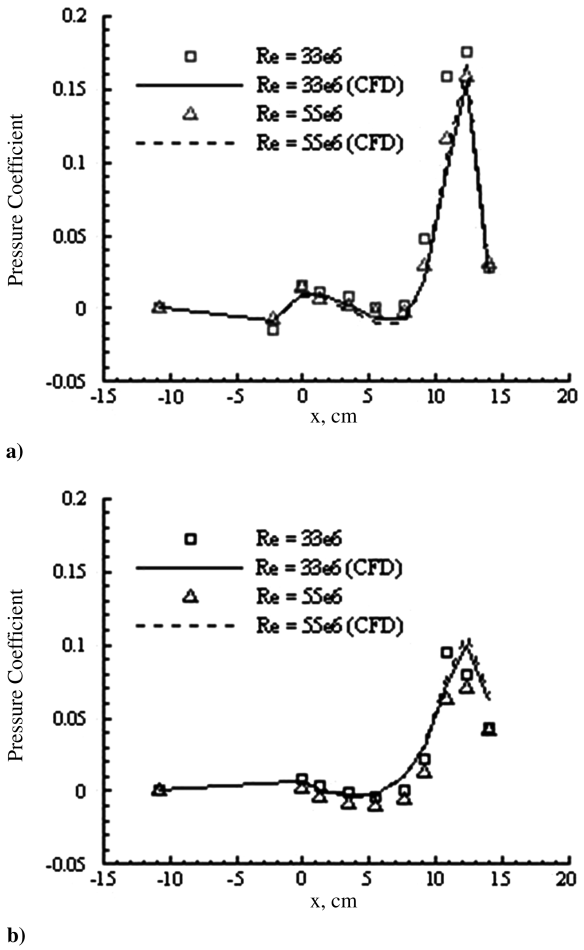


**Fig. 10 Wind-tunnel and CFD centerline surface pressures coefficients at $Re \approx 33 \times 10^6$ m$^{-1}$ and $55 \times 10^6$ m$^{-1}$: a) without pylon and b) with pylon.**

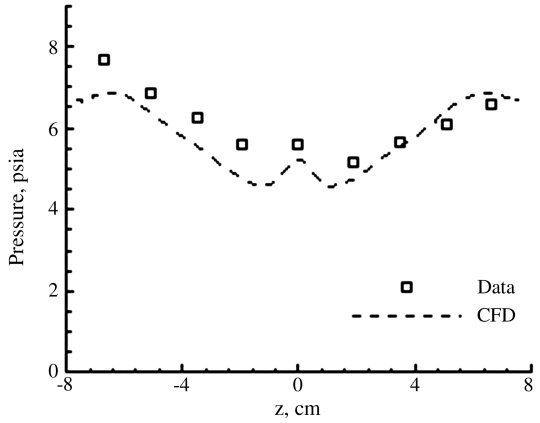


**Fig. 11 Cross-ramp pressures near shear-layer impingement ($x$= 10.8 cm, $y = -0.94$ cm, and $Re \approx 33 \times 10^6$ m$^{-1}$).**

pressure on the ramp in these regions reaches approximately 20% of the stagnation pressure value and signifies potential hot spots in a reacting flow. In reacting flow, however, the shear layer will rise up [24], relieving these high-pressure zones somewhat and spreading the effects across the ramp, reducing their potential local severity. Surface pressure data from the wind tunnel near the shear-layer impingement validate the pressure rise on either side of the cavity ramp (Fig. 11). The skewness in the pressure data across the ramp in Fig. 11 is likely due to small imperfections in test-section construction on the $-z$ wall, as described in [31].

CFD allowed exploration of overall total pressure effects that would be difficult to perform in the wind tunnel. The mass average total pressure ratio for the baseline case was approximately 97.9%, measured from the test-section entrance ($x = -12$ cm) to behind the cavity ($x = 15$ cm). Installing the pylon decreased the ratio to approximately 96.5%, although redesigning the pylon for minimum losses should regain some of the lost total pressure. Changing Reynolds number had negligible effect on total pressure loss. Total pressure data presented in [28] for three different pylon geometries in a reacting flow indicated that a geometry similar to the one tested in this study had less total pressure loss than two other pylon geometries tested. A promising direction for future research would be to identify what pylon dimensions would result in negligible total pressure loss, as described in [33], while still providing a means of carrying cavity products into contact with the main flow.

### C. Flowfield Data

The primary flowfield characteristic of interest is the upward flow of cavity fluid behind the pylon and into contact with the main flow. The computational results shown in Fig. 12 clearly show a strong flow through the low-pressure region behind the pylon from the cavity and into the main flow (approximately $M = 1$ at 1 cm behind

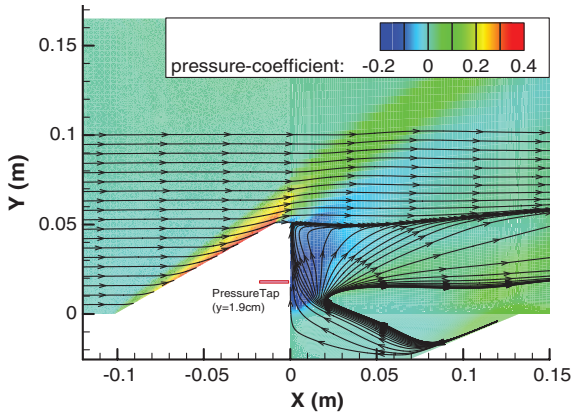


**Fig. 12 CFD centerline pressure coefficient with streamlines ($Re \approx$ 33 x 10$^6$ m$^{-1}$).**

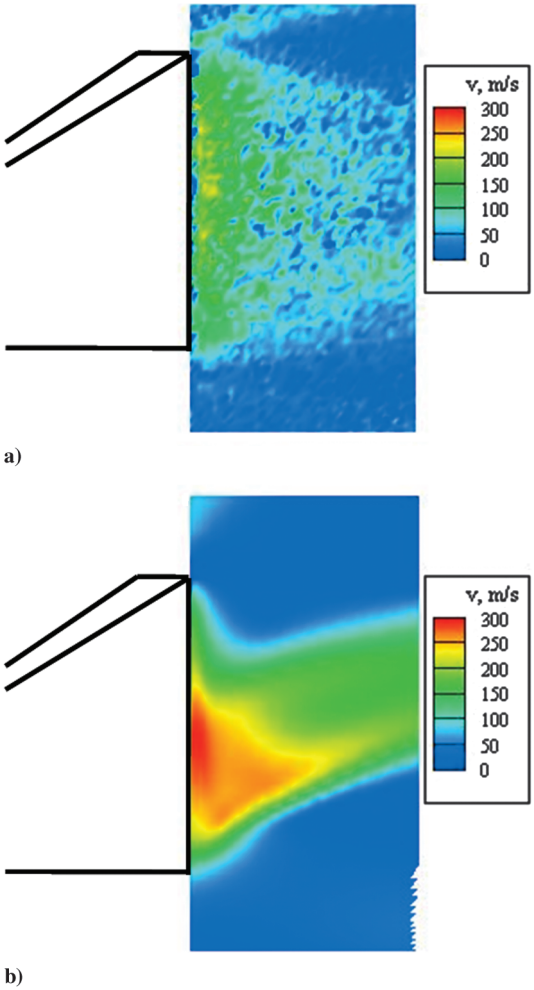


**Fig. 13 Upward velocity on the centerline: a) PIV data, b) CFD data ($Re \approx 33 \times 10^6$ m$^{-1}$ and flow is from the left).**

the downstream face of the pylon at $y = 1.9$ cm). Supersonic expansion behind the pylon and the resulting low static pressure induce the upward flow. The pressure coefficient measured behind the pylon pressure tap at $y = 1.9$ cm was approximately $-0.16$ at all Reynolds numbers and supported computational results. The computational pressure coefficient and upward velocity behind the pylon varied less than 3% over the Reynolds number range used in this study. The upward flow out of the cavity associated with the pylon wake was mostly confined to the base region immediately downstream of the pylon on the centerline, ranging from the tunnel floor to the top of the pylon ($y = 5$ cm) and downstream approximately 2 cm (or about twice the pylon width). Combustion studies using direct cavity injection [28] suggest that reacting products travel to approximately the top of a leading-edge pylon ($h/D = 1.5$), supporting the current study. In contrast, wall fuel injection behind a small pylon ($h/D = 0.6$) upstream of a cavity flameholder had significantly higher penetration into the main flow (more than twice the pylon height) [9], but with more than 10% additional total pressure loss when compared with the current study.

PIV results for vertical velocity, shown in Fig. 13a, show the upward flow behind the pylon. These results are qualitative because to seed the cavity for PIV, an injector was placed along the cavity floor, disrupting the normal flow within the cavity, as did the added mass flow from the $CO_2$ injector in the cavity. These PIV results demonstrate that upward flow behind the pylon does not strictly depend on undisturbed flow within the cavity. For comparison, Fig. 13b shows the computed upward velocity behind the pylon for undisturbed flow.

Figure 14 shows that the pylon wake induces an expansion and recompression shock behind the pylon that could further improve

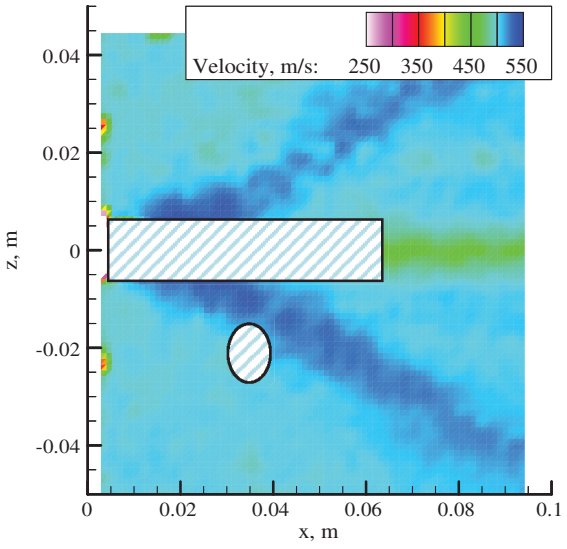


a)

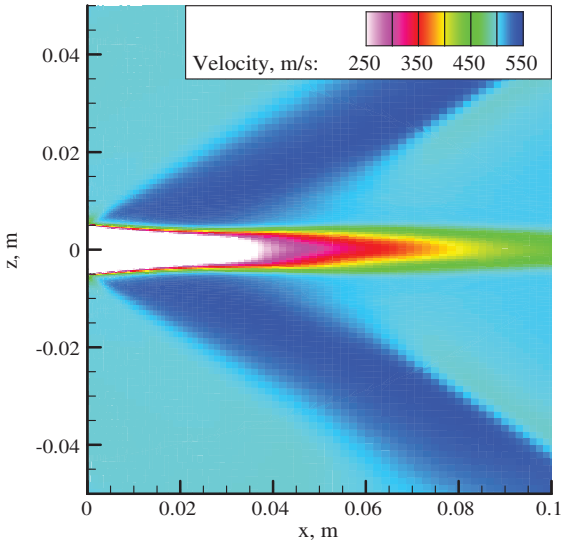


b)

**Fig. 14 Wake flow 3.7 cm above the cavity: a) PIV data, b) CFD data ($Re \approx 33 \times 10^6$ m$^{-1}$, flow is from the left, and the hatched area is unusable data due to low particle density and surface reflections).**

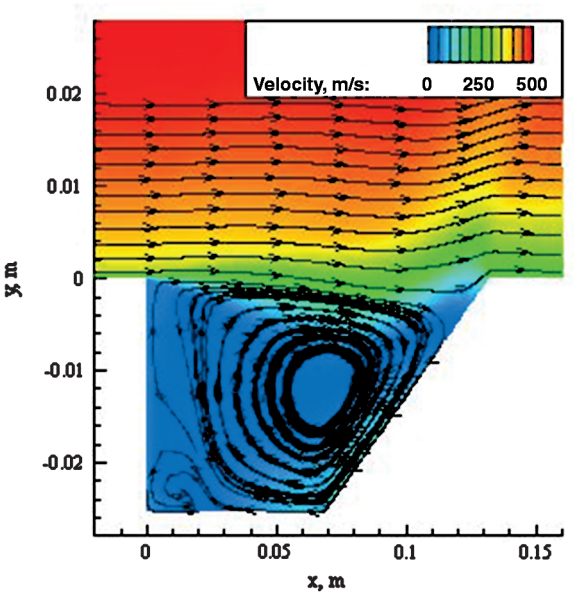


a)

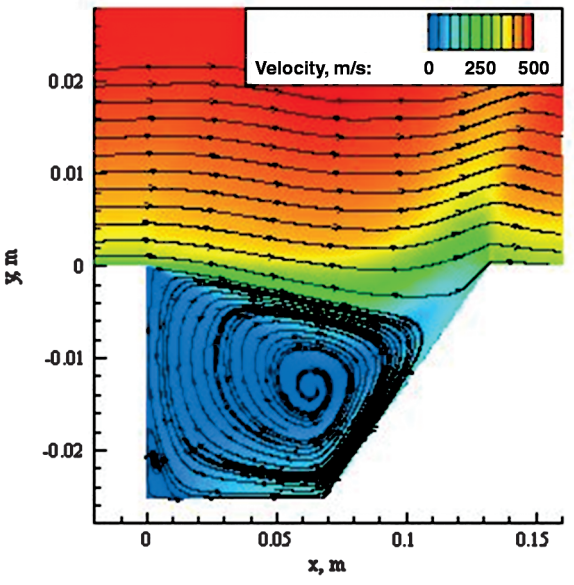


b)

**Fig. 15 CFD streamlines off the cavity centerline ($z = 4$ cm) at $Re = 33 \times 10^6$ m$^{-1}$: a) without pylon and b) with pylon (vertical axis exaggerated).**

mixing with the main flow, as described in [36]. Small differences in overall velocity passing the pylon in the computational data resulted from the different stagnation-tank temperatures used to initialize the simulations. PIV seeding in the pylon wake was extremely sparse, resulting in unreliable wake velocities. However, as seen in Fig. 14, the CFD and PIV data agree on the overall shock and expansion structure behind the pylon. Recompression shock angles agree very well at approximately 33 deg for both CFD and PIV. Contributing to the effectiveness of carrying flameholder products from the cavity into the pylon wake, computational results indicate that the lower vortices seen earlier in Fig. 8 grow and descend along the sides of the pylon wake. These streamwise vortices exchange fluid inside the wake with fluid outside the wake. Assuming that there is combustion within the pylon wake and a suitable fuel–air mixture in the oncoming main flow, the pylon wake will provide a promising means of igniting the oncoming fuel–air mixture. The steady-state single-species computational method precluded the collection of any mixing data; therefore, quantifying the degree of mixing between reacting cavity products and the main flow will require further investigation.

Both the baseline cavity and the pylon cavity had a large vortex oriented across the cavity ($z$ axis) shown in Fig. 15 for $z = 4$ cm. However, unlike the cavity-only case, the cavity flow was split into two regions by the pylon flow effects, as shown in Fig. 16b. In the pylon-cavity case, the flow below the pylon wake inside the cavity was generally upstream (negative $x$ direction) and upward (positive $y$ direction), as seen in Fig. 12. The offcenterline flow behavior of the pylon-cavity model (Fig. 15b) appears to be similar to the cavity-only model (Fig. 15a) and is consistent with previous cavity-only studies [6,11,17,23,24]; that is, the cavity flow was dominated by a large vortex oriented across the cavity (oriented in the $z$ direction). However, the addition of the pylon led to the vortex filling most of the cavity. Without the pylon, the offcenterline vortex was confined to the downstream 75% of the cavity, with lower speed flow dominating the upstream portion. The reverse-flow velocity across the bottom of the downstream ramp with the pylon installed (Fig. 15b) was approximately 155 m/s or about 32% of freestream velocity. Without the pylon (Fig. 15a), the velocity was about 130 m/s or about 26% of freestream velocity. For comparison, [56] presented reverse-flow velocities approximately 40% of freestream in a rectangular cavity. The velocity magnitude down the ramp varied less

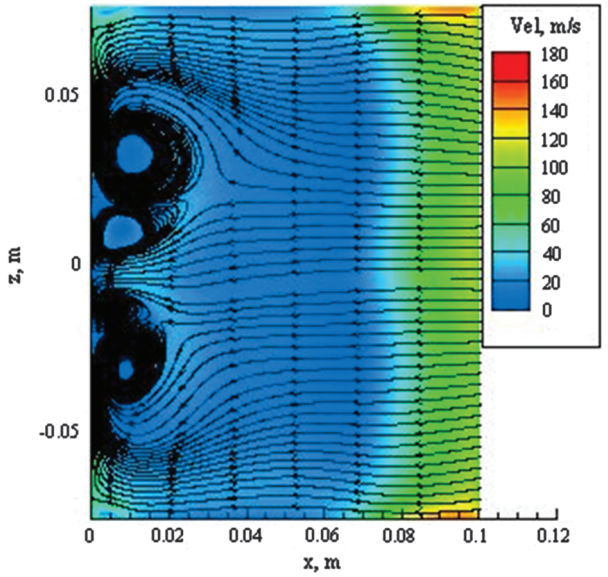


a)

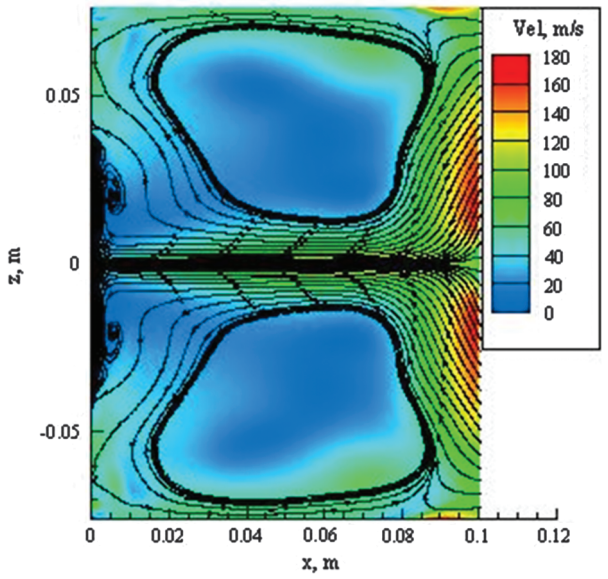


b)

**Fig. 16 CFD streamlines in the cavity midplane: a) without pylon and b) with pylon ($y = -1.27$ cm and $Re \approx 33 \times 10^6$ m$^{-1}$).**

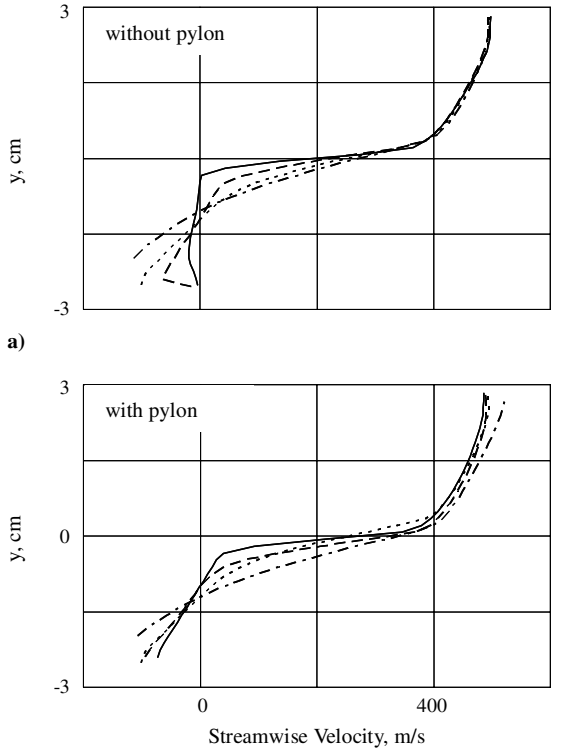


a)

b)

**Fig. 17 CFD streamwise velocity profiles off cavity centerline corresponding to Fig. 15 ($z = 4$ cm) at $Re = 33 \times 10^6$ m$^{-1}$: a) without pylon and b) with pylon $x = 2$ cm (solid line), $x = 4$ cm (dashed line), $x = 6$ cm (dotted line), and $x = 8$ cm (dashed-dotted line).**

than 4% with Reynolds number. The offcenterline ($z = 4$ cm) streamwise velocity profiles in Fig. 17 show that the velocity profiles above the cavity ($y > 0$ cm) are more uniform without the pylon (Fig. 17a) than with the pylon installed (Fig. 17b) and are consistent with $M = 3$ inclined-cavity data in [57]. Figure 17b also indicates that the shear layer drops lower into the cavity and shows the higher reverse-flow velocity with the pylon installed.

In the cavity midplane ($y = -1.27$ cm) seen in Fig. 16, large counter-rotating vortices oriented with the $y$ axis dominate the flow on either side of the pylon wake (Fig. 16b). These regions promote the flow moving upstream and upward beneath the pylon wake and streamwise and downward along the tunnel walls. This pair of vortices defines regions of relatively slow-moving flow. In the cavity-only case (Fig. 16a), the vortices are confined to the upstream wall of the cavity. The local residence time within these vortices should be relatively high, and, assuming a suitable fuel–air mixture is entrained into them, may provide a relatively still environment for stable flameholding. Velocity profiles, shown in Fig. 18, show that the upstream flow without the pylon is strongest along the walls of the cavity and over the ramp (Fig. 18a, $x = 8$ cm). In contrast, with the pylon installed (Fig. 18b), the upstream flow is concentrated on the centerline and a strong flow is maintained over the length of the cavity. The interaction of the low-velocity regions with the fast-moving upstream flow beneath the pylon wake may enable a pool of reacting flameholder products to form and be carried upward behind the pylon and into contact with the main combustor flow.

In summary, the flow features associated with adding a pylon to a cavity flameholder have both positive and negative aspects. The flow is more three-dimensional than the cavity-only case, as exemplified by the mass drawn up behind the pylon. Additionally, whereas the vortices in the cavity increase the mass exchanged between different areas of the flameholder and the main flow, some vortices in the cavity, such as at the bottom of the front cavity wall or either side of the pylon wake, may entrap fuel and be too rich for combustion. These effects may define the limits on flameholder effectiveness, although direct air injection may expand the envelope [6,17,24,58].

### D. Mass Exchange

Addition of the pylon to the leading edge of the cavity should enable greater exchange of mass between the freestream flow and the cavity. This additional mass will be available to react within the cavity and return to the main flow through the pylon wake or downstream edge of the cavity. The average mass flow passing from the main flow through the cavity and back into contact with the main flow either through the pylon wake or at the downstream cavity ramp was computationally estimated by integrating the positive mass flow per unit area across the top of the cavity:

$$\dot{m}_{\text{cav}} = \left[ \int_A \rho u_{y_+} \, \mathrm{d}A \right]_{y=0} \tag{3}$$

where $\rho$ is the local cell density and $u_{y+}$ is the positive component of vertical velocity. The calculation only requires the positive component because the mean mass flow into the cavity and out of the cavity will be the same (the difference between positive and

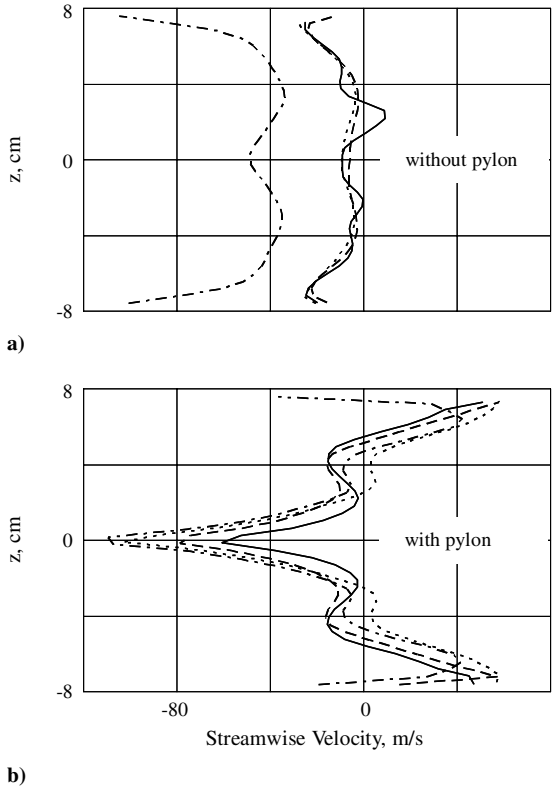


**Fig. 18 CFD streamwise velocity profiles across the cavity midplane corresponding to Fig. 17 ($y = -1.27$ cm and $Re \approx 33 \times 10^6$ m$^{-1}$): a) without pylon and b) with pylon $x = 2$ cm (solid line), $x = 4$ cm (dashed line), $x = 6$ cm (dotted line), and $x = 8$ cm (dashed-dotted line).**

negative mass flow CFD solutions through the top of the cavity is less than 1%).

The pylon-cavity case is very three-dimensional, with the previously discussed flow structures mechanically driving much of the mass exchange. In contrast, the cavity-only case has significantly less interaction between the cavity flow and freestream. Because a steady-state CFD calculation cannot reliably predict cavity residence time, the mass flow ratio (MFR) provides a better comparison between pylon and no-pylon cases (i.e., the proportion of freestream mass flow that passes through the cavity):

$$\text{MFR} = \dot{m}_{\text{cav}}/\dot{m}_{\text{freestream}} \tag{4}$$

The mass flow ratio of the pylon-cavity case was approximately 0.012 for all Reynolds numbers (i.e., slightly over 1% of the mass flow transits the cavity). Without the pylon, the mass flow fraction was 0.004 for all Reynolds numbers, or about one-third the cavity mass flow of the pylon cavity. Assuming fuel injection upstream of the flameholder, 3 times more fuel–air mixture passes through the cavity and back into contact with the freestream per unit time with the pylon added to the leading edge. As described in [17], increasing cavity length also increases the mass exchange with the freestream. However, the addition of a pylon significantly alters the cavity flowfield and produces more intense three-dimensional effects than lengthening the cavity. Cavity-only mass flows approximated using [17] data showed a modest increase (approximately 15%) when increasing cavity $L/D$ from three to five as opposed to the approximately 300% increase from the addition of the pylon used in this study. Note that these characteristics would obviously change in the case of direct cavity injection of fuel and/or air. MFR, as calculated through the top of the cavity, does not provide an estimate of mixing, but indicates a relative measure of cavity products available to interact with the main flow through the cavity shear layer and pylon wake. Future research should investigate the effects on fuel–air mixing and component efficiency. Also, MFR presents only the mean mass flow through the top of the cavity and fails to account for significant local differences. For instance, in the middle of the relatively still flow on either side of the cavity, as seen in Fig. 16b, the local residence time will be relatively high.

In general, increased mass exchange can be beneficial in terms of exposing more reacting flameholder products to the main flow. However, the inverse relationship between mass exchange and residence time requires care to ensure that mass exchange does not increase beyond the capability of the flameholder to sustain combustion. If necessary, increasing the cavity depth, and therefore volume, should increase overall residence time. As described in [17], the flameholder mass exchange will decrease in a reacting flow with the resulting increased residence time. Therefore, the cold-flow relationships noted in this study are conservative with regard to mean residence time/MFR.

## VI. Conclusions

This paper presents results of a combined experimental/computational study of an inclined-cavity flameholder with a swept-leading-edge pylon and should help bound part of the design problem facing a scramjet engine designer opting to use a pylon-cavity flameholder. The test conditions were a Mach number of 2 and unit Reynolds numbers between approximately $33 \times 10^6$ m$^{-1}$ and $55 \times 10^6$ m$^{-1}$.

The low pressure resulting from the expansion around the back of the pylon led to a strong flow upward from the cavity. This upward flow into the pylon wake increased mass exchange between the main flow and the cavity, compared with the cavity-only case. The larger mixing area of the pylon wake combined with the cavity shear layer provided a larger interface for pylon-cavity flameholder products to interact with the oncoming fuel–air mixture than a cavity-only configuration. These effects provide an avenue for the reacting products in the cavity to extend at least as far as the top of the pylon wake and higher into the main flow than either a cavity-only or step design. Although research must continue, knowledge of the flow features discussed in this paper should assist in improving fuel–air injector designs for use in a pylon-cavity flameholder and provide a stepping stone toward optimizing the pylon-cavity configuration, with the ultimate goal of improving overall combustor performance.

## Acknowledgments

The authors thank John Hixenbaugh and Jay Anderson for their laboratory support, Mark Reeder and Bartt Greene for their assistance with the $CO_2$ clean-seeding method for particle image velocimetry, and Raymond Maple for his assistance in preparing the computational fluid dynamics evaluation.

## References

[1] Canan, J. W., "Breathing New Hope into Hypersonics," *Aerospace America*, Vol. 45, No. 11, 2007, pp. 26–31.

[2] Taverna, M. A. and Barrie, D., "India Eyes Hyper-Cruise," *Aviation Week and Space Technology*, Vol. 167, No. 18, 2007, p. 65.

[3] Wilson, J. R., "High Hopes for HIFiRE Scramjet," *Aerospace America*, Vol. 45, No. 11, 2007, pp. 32–37.

[4] Norris, G., "All Fired Up," *Aviation Week and Space Technology*, Vol. 168, No. 18, 2008, p. 42.

[5] Butterworth-Hayes, P., "Europe Speeds Up Hypersonic Research," *Aerospace America*, Vol. 46, No. 6, 2008, pp. 24–28.

[6] Edens, S. G., "Performance Measurements of Direct Air Injection in a Cavity-Based Flameholder for a Supersonic Combustor," M.S. Thesis, Dept. of Aeronautics and Astronautics, Air Force Inst. of Technology, Wright–Patterson AFB, OH, 2006.

[7] Montes, D. R., King, P. I., Gruber, M. R., and Hsu, K., "Mixing Effects of Pylon-Aided Fuel Injection Located Upstream of a Flameholding Cavity in Supersonic Flow," AIAA Paper 2005-3913, July 2005.

[8] Haubelt, L. C., "Supersonic Loss and Mixing Over A Cavity Flame Holder Located Downstream of Pylon-Aided Fuel Injection," M.S. Thesis, Dept. of Aeronautics and Astronautics, Air Force Inst. of Technology, Wright–Patterson AFB, OH, 2006.

[9] Gruber, M. R., Carter, C. D., Montes, D. R., Haubelt, L. C., King, P. I., and Hsu, K., "Experimental Studies of Pylon-Aided Fuel Injection into a Supersonic Crossflow," *Journal of Propulsion and Power*, Vol. 24, No. 3, 2008, pp. 460–470.
doi:10.2514/1.32231

[10] Ben-Yakar, A., and Hanson, R. K., "Cavity Flame-Holders for Ignition and Flame Stabilization in Scramjets: An Overview," *Journal of Propulsion and Power*, Vol. 17, No. 4, 2001, pp. 869–877. doi:10.2514/2.5818
[11] Gruber, M. R., Donbar, J. M., Carter, C. D., and Hsu, K., "Mixing and Combustion Studies Using Cavity-Based Flameholders in a Supersonic Flow," *Journal of Propulsion and Power*, Vol. 20, No. 5, 2004, pp. 769–777. doi:10.2514/1.5360
[12] Glassman, I., *Combustion*, 3rd ed., Academic Press, San Diego, 1996.
[13] Yu, K. H., Wilson, K. J., and Schadow, K. C., "Effect of Flame-Holding Cavities on Supersonic-Combustion Performance," *Journal of Propulsion and Power*, Vol. 17, No. 6, 2001, pp. 1287–1295. doi:10.2514/2.5877
[14] Tam, C. J., Orkwis, P. D., and Disimile, P. J., "Algebraic Turbulence Model Simulations of Supersonic Open-Cavity Flow Physics," *AIAA Journal*, Vol. 34, No. 11, 1996, pp. 2255–2260. doi:10.2514/3.13388
[15] Rizzetta, D. P., "Numerical Simulation of Supersonic Flow Over a Three-Dimensional Cavity," *AIAA Journal*, Vol. 26, No. 7, 1988, pp. 799–807. doi:10.2514/3.9972
[16] Rossiter, J. E., "Wind-Tunnel Experiments on the Flow over Rectangular Cavities at Subsonic and Transonic Speeds," Aeronautical Research Council, Reports and Memoranda No. 3438, 1964.
[17] Gruber, M. R., Baurle, R. A., Mathur, T., and Hsu, K., "Fundamental Studies of Cavity-Based Flameholder Concepts for Supersonic Combustors," *Journal of Propulsion and Power*, Vol. 17, No. 1, 2001, pp. 146–153. doi:10.2514/2.5720
[18] Davis, D. L., "Numerical Analysis of Two and Three Dimensional Recessed Flame Holders for Scramjet Applications," Ph.D. Dissertation, Dept. of Aeronautics and Astronautics, Air Force Inst. of Technology, Wright–Patterson AFB, OH, 1996.
[19] Jeong, E., O'Byrne, S., Jeung, I., and Houwing, A. F. P., "Cavity Flame-Holder Experiments in a Model Scramjet Engine," AIAA Paper 2006-7918, 2006.
[20] Kim, C., Yu, S. J., and Zhang, Z., "Cavity Flow in Scramjet Engine by Space-Time Conservation and Solution Element Method," *AIAA Journal*, Vol. 42, No. 5, 2004, pp. 912–919. doi:10.2514/1.9017
[21] Rasmussen, C. C., Driscoll, J. F., Carter, C. D., and Hsu, K., "Characteristics of Cavity-Stabilized Flames in a Supersonic Flow," *Journal of Propulsion and Power*, Vol. 21, No. 4, 2005, pp. 765–768. doi:10.2514/1.15095
[22] Drummond, J. P., Carpenter, M. H., and Riggins, D. W., "Mixing and Mixing Enhancement in Supersonic Reacting Flowfields," *High-Speed Flight Propulsion Systems*, edited by Murthy, S. N. B. and Curran, E. T., Progress in Aeronautics and Astronautics, AIAA, Washington DC, 1991, pp. 265–340.
[23] Baurle, R. A., Gruber, M. R., "A Study of Recessed Cavity Flowfields for Supersonic Combustion Applications," AIAA Paper 98-0938, Jan 1998.
[24] Allen, W. H., "fuel–air Injection Effects on Combustion in Cavity-Based Flameholders in a Supersonic Flow," M.S. Thesis, Dept. of Aeronautics and Astronautics, Air Force Inst. of Technology, Wright–Patterson AFB, OH, 2005.
[25] Seiner, J. M., Dash, S. M., and Kenzakowski, D. C., "Historical Survey on Enhanced Mixing in Scramjet Engines," *Journal of Propulsion and Power*, Vol. 17, No. 6, 2001, pp. 1273–1286. doi:10.2514/2.5876
[26] Owens, M., Tehranian, S., Segal, C., and Vinogradov, V., "Flame-Holding Configurations for Kerosene Combustion in a Mach 1.8 Airflow," *Journal of Propulsion and Power*, Vol. 14, No. 4, 1998, pp. 456–461. doi:10.2514/2.5322
[27] Thakur, A., and Segal, C., "Concentration Distribution in a Supersonic Flow Recirculation Region," *Journal of Propulsion and Power*, Vol. 24, No. 1, 2008, pp. 64–73. doi:10.2514/1.25396
[28] Hsu, K., Carter, C. D., Gruber, M. R., and Barhorst, T., "Experimental Study of Cavity-Strut Combustion in Supersonic Flow," AIAA Paper 2007-5394, July 2007.
[29] Freeborn, A. B., King, P. I., and Gruber, M. R., "Characterization of Pylon Effects on a Scramjet Cavity Flameholder Flowfield," AIAA Paper 2008-0086, Jan 2008.
[30] Freeborn, A. B., King, P. I., and Gruber, M. R., "Leading Edge Pylon Effects on a Scramjet Pylon-Cavity Flameholder Flowfield," AIAA Paper 2008-4709, July 2008.
[31] Freeborn, A. B., "Pylon Effects on a Scramjet Cavity Flameholder Flowfield," Ph.D. Dissertation, Air Force Inst. of Technology, Dept. of Aeronautics and Astronautics, Wright–Patterson AFB, OH, 2008.
[32] Bogdanoff, D. W., "Advanced Injection and Mixing Techniques for Scramjet Combustors," *Journal of Propulsion and Power*, Vol. 10, No. 2, 1994, pp. 183–190. doi:10.2514/3.23728
[33] Vinogradov, V., Shikhman, Y., and Segal, C., "A Review of Fuel Pre-Injection in Supersonic, Chemically Reacting Flows," *Applied Mechanics Reviews*, Vol. 60, July 2007, pp. 139–148. doi:10.1115/1.2750346
[34] Anderson, J. D., *Modern Compressible Flow with Historical Perspective*, 3rd ed., McGraw Hill, New York, 2003.
[35] Riggens, D. W., and Vitt, P. H., "Vortex Generation and Mixing in Three-Dimensional Supersonic Combustors," *Journal of Propulsion and Power*, Vol. 11, No. 3, 1995, pp. 419–426. doi:10.2514/3.23860
[36] Heiser, W. H., and Pratt, D. T., *Hypersonic Airbreathing Propulsion*, AIAA, Washington, DC., 1994.
[37] Gruenig, C., Avrashkov, V., and Mayinger, F., "Fuel Injection into a Supersonic Airflow by Means of Pylons," *Journal of Propulsion and Power*, Vol. 16, No. 1, 2000, pp. 29–34. doi:10.2514/2.5560
[38] Fuller, R., Wu, P., Nejad, and, Schetz, A.,"Comparison of Physical and Aerodynamic Ramps as Fuel Injectors in Supersonic Flow," *Journal of Propulsion and Power*, Vol. 14, No. 2, 1998, pp. 135–145. doi:10.2514/2.5278
[39] Vinogradov, V., Kobigsky, S., and Petrov, M., "Experimental Investigation of Kerosene Fuel Combustion in Supersonic Flow," *Journal of Propulsion and Power*, Vol. 11, No. 1, 1995, pp. 130–134. doi:10.2514/3.23850
[40] Vinogradov, V., Shikhman, Y., Albegov, R., and Vedeshkin, G., "Experimental Research of Pre-Injected Methane Combustion in High Speed Subsonic Airflow," AIAA Paper 2003-6940, 2003.
[41] Ortwerth, P., Mathur, A., Vinogradov, V., Grin, V., Goldfeld, M., and Starov, A., "Experimental and Numerical Investigation of Hydrogen and Ethylene Combustion in a Mach 3-5 Channel with a Single Injector," AIAA Paper 96-3245, 1996.
[42] Gu, H., Chen, L., and Chang, X., "Experimental Investigation of Cavity-based Scramjet Model," AIAA Paper 2006-7917, 2006.
[43] Arai, T., Sakaue, S., Morisaki, T., Kondo, A., Hiejima, T., and Nishioka, M., "Supersonic Streamwise Vortices Breakdown in Scramjet Combustor," AIAA Paper 2006-8025, 2006.
[44] Amick, J. L., Liepman, H. P., and Reynolds, T. H., "Development of a Variable Mach Number Sliding Block Nozzle and Evaluation in the Mach 1.3 to 4.0 Range," WADC Wright Air Development Center, Technical Report 55-88, March 1955.
[45] "Operating Instructions for WPAFB 6″ by 6″ Supersonic Wind Tunnel," Aerolab, Mar. 1996.
[46] DeLapp, C. J., "Particle Image Velocimetry Using Novel, Non-Intrusive Particle Seeding," M.S. Thesis, Dept. of Aeronautics and Astronautics, Air Force Inst. of Technology, Wright–Patterson AFB, OH, 2006.
[47] DeLapp, C. J., and Reeder, M. F., "Clean Seeding Material for Particle Image Velocimetry Measurements," AIAA Paper 2006-2807, 2006.
[48] McNiel, C. M., "Demonstration of Clean Particle Seeding For Particle Image Velocimetry in a Closed Circuit Supersonic Wind Tunnel," M.S. Thesis, Dept. of Aeronautics and Astronautics, Air Force Inst. of Technology, Wright–Patterson AFB, OH, 2007.
[49] Peltier, D. W., III, "Performing Particle Image Velocimetry in a Supersonic Wind Tunnel Using Carbon Dioxide as the Seed Material," M.S. Thesis, Dept. of Aeronautics and Astronautics, Air Force Inst. of Technology, Wright–Patterson AFB, OH, 2007.
[50] Greene, B. G., "Characterization and Control of Carbon Dioxide Seed Particles in Particle Image Velocimetry," M.S. Thesis, Dept. of Aeronautics and Astronautics, Air Force Inst. of Technology, Wright–Patterson AFB, OH, 2008.
[51] Greene, B. G., Reeder, M. F., and Crafton, J., "Characterizing Dry Ice Particle Response for Clean Seeding PIV Applications," AIAA Paper 2008-3714, 2008.
[52] Menter, F. R., "Two-Equation Eddy-Viscosity Turbulence Models for Engineering Applications," *AIAA Journal*, Vol. 32, No. 8, 1994, pp. 1598–1605. doi:10.2514/3.12149
[53] Gabruk, R. S., and Roe, L. A., "Velocity Characteristics of Reacting and Nonreacting Flows in a Dump Combustor," *Journal of Propulsion and Power*, Vol. 10, No. 2, 1994, pp. 148–154. doi:10.2514/3.23723
[54] Barber, T. J., and Anderson, O. L., "Computational Study of a

Supersonic Mixer-Ejector Exhaust System," *Journal of Propulsion and Power*, Vol. 8, No. 5, 1992, pp. 927–934.
doi:10.2514/3.23574

[55] Holman, J. P., and Gajda, W. J., *Experimental Methods for Engineers*, 5th ed., McGraw-Hill, New York, 1989.

[56] Zhuang, N., Alvi, F. S., Alkislar, M. B., and Shih, C., "Supersonic Cavity Flows and Their Control," *AIAA Journal*, Vol. 44, No. 9, 2006, pp. 2118–2128.
doi:10.2514/1.14879

[57] Horstman, C. C., Settles, G. S., Williams, D. R., and Bogdanoff, S. M., "A Reattaching Free Shear Layer in Compressible Turbulent Flow," *AIAA Journal*, Vol. 20, No. 1, 1982, pp. 79–85.
doi:10.2514/3.51049

[58] Allen, W., King, P. I., Gruber, M. R., Carter, C. D., and Hsu, K., "fuel–air Injection Effects on Combustion in Cavity-Based Flameholders in a Supersonic Flow," AIAA Paper 2005-4105, 2005.

C. Segal
*Associate Editor*